THE SAO SUBMILLIMETER WAVELENGTH ARRAY

JAMES M. MORAN
Center for Astrophysics, 60 Garden St., Cambridge, MA 02138

Abstract. The SAO Submillimeter Wavelength Array is under construction and is expected to be ready for observations in 1997. It will consist of six telescopes with baselines from 9 to 470 m and resolutions as fine as 0.″1. Eight receivers will cover all bands from 180 to 900 GHz in linear polarization; two orthogonal polarizations will be available at 350 GHz. Multiyear site testing on Mauna Kea shows that the precipitable water vapor is less than 1 mm for 17% of the time, and the rms phase fluctuations on a baseline of 100 m are less than 55μm for 25% of the time. The configuration of the array will be optimized to provide nearly uniform coverage in the uv plane. The correlator spectrometer will have 10^5 spectral channels (8192 per baseline) and will be able to provide 0.6 MHz resolution for a total bandwidth of 4 GHz.

1. INTRODUCTION

The Smithsonian Astrophysical Observatory (SAO) is constructing an interferometric array for imaging observations at submillimeter wavelengths. The basic characteristics of the Submillimeter Array (SMA) are listed in Table 1. Initial funding for the project began in 1989 and first operation is planned for 1997. Detailed descriptions of the project can be found in Moran et al (1984) and Masson et al (1992). The submillimeter band (300–900 GHz; 1 mm–0.35 mm) offers formidable difficulties for ground-based operation because of the opacity of the atmosphere. However substantial progress has been made with low resolution telescopes as the receiver technology has improved (e.g., Phillips and Keene 1992). The operation of an imaging interferometer at submillimeter wavelengths has several advantages. For example, although the collecting area of the proposed array is relatively small, the brightness temperature sensitivity is high, because of the ν^2 dependence of the blackbody law at radio wavelengths. That is

$$\Delta T_B = \left(\frac{c}{\nu}\right)^2 \frac{1}{A\theta^2} \frac{T_S}{\sqrt{\Delta\nu\tau}} \tag{1}$$

where A is the total collecting area of the array, T_S is the system temperature, $\Delta\nu$ is the bandwidth, τ is the integration time, θ is the angular resolution, and c is the velocity of light. The expected brightness temperature sensitivities of the SMA are listed in Table 2. The submillimeter region is rich in important spectral lines of many atomic and molecular species. The emissivity of dust increases as ν^{1-2} so the flux density rises as ν^{3-4}, making the submillimeter band a sensitive place to study its properties. However, the dust is still generally optically thin, so measurements of column densities can be made.

2. SCIENTIFIC APPLICATIONS

The high angular and spectral resolution of the array will make it possible to study the dynamical properties of material around forming stars. For example, in a star forming region such as Ophiuchus (~100 pc distant), 1″ resolution corresponds to 10^{15} cm where the free fall speed is 4 km s^{-1} for a 1 $M_\odot$ core, considerably greater

J.G. Robertson and W.J. Tango (eds.), Very High Angular Resolution Imaging, 27–35.

Table 1 Array Characteristics

Elements	
number/diameter	6 × 6 m
surface accuracy	12μm
construction features	alt-az mount, carbon fiber backup structure, cast aluminum panels, Nasmyth focus, primary reflector f/0.4
array configuration	4 concentric rings with 6 pads each
baselines	9–460 m
operating frequencies	180 GHz–900 GHz
maximum resolution	0.4″ –0.1″
field of view	54″ –15″
number of receivers	8 (2 simultaneous)
IF	4–6 GHz (2 GHz for each of 2 receivers)
correlator	Digital FX; 10^5 effective channels; 0.6 MHz resolution at full bandwidth
maximum data rate	0.7 Gbyte/day
cost	$45M

Table 2 Sensitivity of the SMA[1]

Frequency (GHz)	Ts[2] (K)	Field of view[3] (″)	Resolution[4] (″)	ΔT[5] (K)	ΔT[6] (K)	ΔS[6] (mJy)
230	210	54	9	0.01	0.0003	0.7
			0.4	8	0.2	
345	610	36	6	0.44	0.001	2.2
			0.3	21	0.5	
490	2800	25	4.2	0.1	0.004	10
			0.2	82	2.3	
820	13200	15	2.5	0.5	0.02	43
			0.1	260	10	

[1] Noise levels are 1σ values, based on an integration time of 8 hours and include a receiver loss factor of 1.05 and a digital processing loss factor of 1.15. At 820 GHz there is an extra loss factor of 2.0 for optical coupling.
[2] SSB system temperatures with 1 mm of precipitable water and 1.5 air masses. The (SSB) receiver temperatures are 120, 300, 400 and 1500K respectively.
[3] The full primary beamwidth of 6-m element.
[4] Resolution for 21 m and 470 m configurations. The sensitivities for the intermediate arrays of length 60 and 160 m can be calculated by use of equation (1).
[5] Rayleigh-Jeans equivalent noise level at 1 km/s resolution.
[6] Noise level for 2 GHz bandwidth.

https://doi.org/10.1017/S0074180900107296 Published online by Cambridge University Press

than the normal turbulent velocity of $\sim$1 km s^{-1}. Hence it should be possible to detect gravitational infall around forming stars and to study their accretion disks. High resolution continuum measurements of dust will also be important for star formation studies (e.g., Mezger et al 1988). The array will be used to study gas and dust in external galaxies and the emission from active galactic nuclei and quasars.

Undoubtedly, many unknown applications will arise for the array. Promising areas include the CII line and masers. The CII line at 158μm is an important coolant in photodissociation regions in galaxies and may account for as much as 1% of their total infrared luminosity. For galaxies with $z = 1 - 5$ this CII line would be redshifted into the submillimeter band and could be studied by the array (e.g., Loeb 1993). Several powerful submillimeter wavelength water vapor masers have been discovered (e.g., Menten 1991) that can be studied or used as phase references.

3. SITE TESTING

Because the atmosphere is only partially transparent at submillimeter wavelengths, the array must be sited at a location with a small amount of water vapor overhead. Other considerations are: low turbulence for good phase stability; low latitude for best sky coverage including high elevation coverage of Orion and Sagittarius regions of the Galaxy; 500 m diameter flat area for siting array; freedom from severe storms and high winds; developed observatory infrastructure; and environmental factors. We have selected a site on Mauna Kea near the CSO and JCMT. Sites in Arizona, California, and northern Chile were also seriously considered.

A very extensive set of site evaluation data has been obtained for Mauna Kea with automated sensors. In collaboration with SAO and CSO, NRAO has operated a tipping radiometer near the CSO telescope for the past three years. The opacity at 225 GHz has been measured every ten minutes and nearly 10^5 observations have been obtained. The results are shown in Figure 1. An opacity of 0.05 at 225 GHz corresponds to 1 mm of precipitable water and to opacities of 0.18 at 345 GHz, and 0.8 at 490, 690 and 820 GHz. The results show that the opacity is 0.05 or less at 225 GHz for 17% of the total time. The lowest opacity can occur at any time of day but the best conditions occur at night. In addition, there is a clear seasonal effect with conditions from January to June being substantially better than from July to December.

Masson (1993a) built a phase monitoring system which has been in operation for two years on Mauna Kea. This instrument consists of two small dishes separated by 100 m, which are used to measure the phase difference of a 12 GHz beacon signal from a geostationary satellite (GStar A2). Since the troposphere is nearly non-dispersive, the measured relative delays at 12 GHz accurately reflect conditions at frequencies up to 1000 GHz. The statistics of the rms fluctuations in relative path length for a 15-minute averaging time are shown in Figure 1. Approximately 25% of the time the path fluctuations are smaller than 55μm on a 100 m baseline or 1 radian at the highest frequency of the SMA. The rms fluctuations are expected to scale as $D^{0.83}$, where D is the baseline length, for Kolmogorov turbulence, but in practice, the power law index, as deduced from the temporal power spectrum,

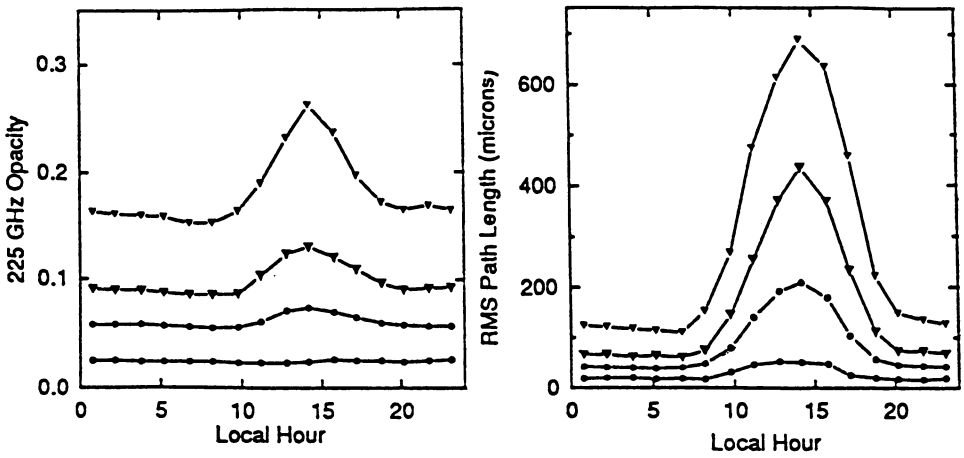

Fig. 1. (left) The opacity on Mauna Kea at 225 GHz as a function of local time; minimum, 25, 50, and 75 percentile values for 1989–1992. An opacity of 0.05 corresponds to 1 mm of precipitable water. (right) Relative rms path length corrected to the zenith direction on a 100 m baseline as function of local time. The atmosphere at frequencies from 10 to 1000 GHz is essentially non-dispersive and the rms phase fluctuation is the RF frequency times the path length fluctuation (Masson 1993a).

appears to be slightly smaller (Masson 1993b). The median value of the limiting resolution is 1.″2 at 345 GHz (scaling as $\nu^{-0.3}$).

Because the absolute temperature changes along through the lower troposphere are small, the sky opacity and path length (integrated index of refraction) are highly correlated (10 μm of precipitable water gives 60 μm path length and 0.15K of sky brightness at 225 GHz). Hence if the sky brightness temperature can be accurately measured, the path length can be corrected. Very stable receivers ($\Delta T/T \sim 10^{-4}$), clear sky, and models for ground pickup are needed. Welch (1993) has demonstrated the feasibility of this technique, which could have a major impact on the quality of images when calibration methods such as closure phase cannot be used.

4. ANTENNAS

The antennas have been designed at SAO and will be fabricated by subcontractors and initially assembled on the grounds of Haystack Observatory. The antennas will operate in the open air without protection. The primary reflector will be a parabola with 6 meter diameter in an alt-azimuth configuration. Elevation motion will be controlled by a linear actuator. The 72 machined aluminum panels comprising the reflector will be arranged in four rings and the position of each panel will be set by four manually controlled actuators. The backup structure will be constructed of carbon fiber struts and steel nodes. The overall error budget for the primary surface is 12 μm (rms). The subreflector will be about 0.35 m in diameter. Three

additional mirrors will be required to bring the signal to the non-tilting receiver cabin which is mounted above the azimuth bearing. The effective focal ratio is 14.

5. ARRAY CONFIGURATION

The optimum layout of an array is a complex problem; it is difficult even to specify the optimization criteria. An EW array with minimum redundant spacings has poor performance on sources near the celestial equator because of the baseline foreshortening in the NS direction (e.g., Thomson, Swenson and Moran 1986). Perhaps the most successful two dimension array is the VLA, with its Y configuration. The elements are spaced at intervals give by a power law and the uv plane coverage is markedly centrally condensed. Cornwell (1988) considered the optimum layout under the condition that the antennas are confined to lie within a *circular area*. The positions were sought that maximized the separations among the uv points (the sum of the logarithms of the uv plane separations was maximized). The antennas moved to the circular boundary and for odd numbers of antennas, the locations were found to lie at the vertices of regular hexagons. Keto (1993) re-examined this problem using a neural network to search for optimum solutions. He required that the uv points be as uniformly distributed as possible within a circular boundary in the *uv plane*. For this condition, the antennas are laid out approximately along the sides of a Reuleaux triangle (Gardner 1968), an equilateral triangle with curved sides where the center of curvature of each side is the opposite vertex. This triangle has constant curvature and is one member of a family of curves with constant width of which a circle is the simplest example. Figure 2 shows the optimum arrays for 6 and 24 antennas. For 6 antennas, the uv distribution is a hexagonal pattern. The Reuleaux triangle is clearly evident for the 24 antenna array. Note that the optimum instantaneous uv coverage at zenith leads to the optimum coverage with earth rotation (see Figure 3).

The SMA will be configured like the six-element array in Figure 2. There will be four concentric rings with 6 pads each. The scale factor among the rings is $\sim$2.8 (21, 60, 160, 470 m). The range of spacings with any one configuration is only about 3:1 in the absence of foreshortening, and about 6:1 for a source at 45° declination (see Figure 3). Hence it will be necessary to combine the data from several arrays to construct images sensitive to structures on a range of scales greater than 6:1. For observations at higher resolution and sensitivity, the CSO and JCMT will be joined to the array.

6. RECEIVERS

The receivers for the array will cover all usable bands from 180 to 900 GHz. A complement of eight receivers are planned to cover the frequency ranges 170–260 GHz (2); 250–350 GHz (2); 330–420 GHz; 400–520 GHz; 620–720 GHz; 800–900 GHz. These receivers will all consist of SIS mixers followed by low noise HEMT IF amplifiers. The current state of the art in SIS receivers is described by Blundell and Tong (1992) and the receiver temperatures of 10 $h\nu/k$ should be achievable. The initial complement of receivers will be the ones covering 230, 345, and 460 GHz.

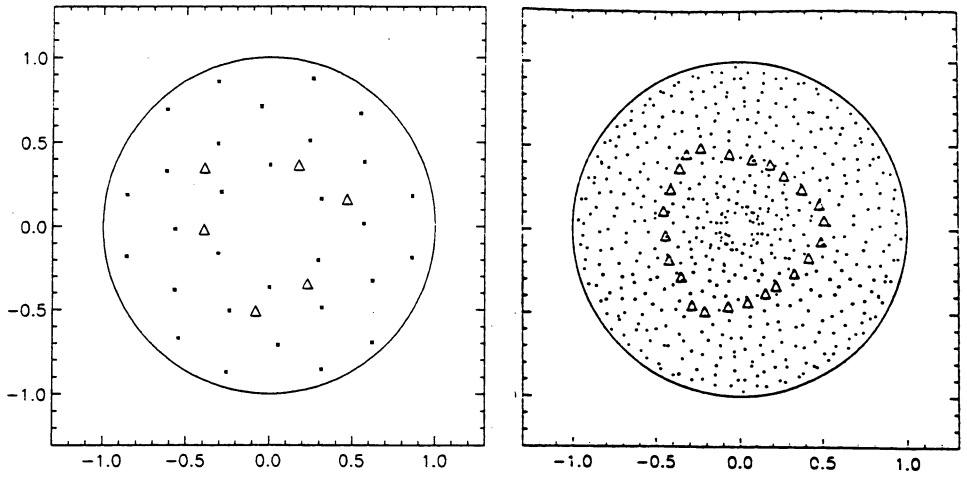

Fig. 2. The optimum array configurations for 6 and 24 elements that provide the most uniform coverage in the uv plane within a circular area. The antenna locations in physical space are denoted by triangles and the uv coverage (or the array autocorrelation function) is denoted by dots. The uv point at the origin is omitted. From Keto (1993).

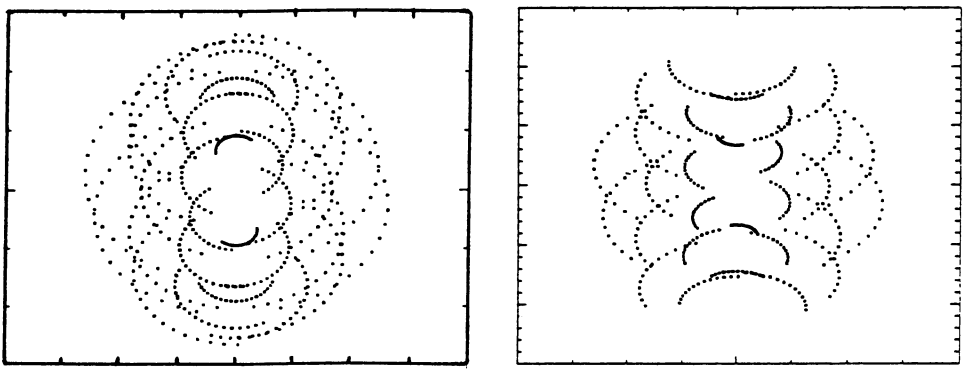

Fig. 3. The uv plane coverage for a source at 45° declination (left) and -28° declination (right) obtained with the six element array in Figure 1 located on Mauna Kea (latitude=19°). From Masson et al (1992).

https://doi.org/10.1017/S0074180900107296 Published online by Cambridge University Press

The mixers for these receivers will be built in waveguides with suspended quartz substrates supporting the superconducting mixer elements, Niobium/Aluminum oxide/Niobium tunnel junctions. For the higher frequency bands, different junction technology may be required since the gap frequency of niobium junctions is about 680 GHz, above which mixing becomes less efficient. The choice between waveguide and quasi-optical designs for the higher frequencies is not clear. The local oscillator signals will be supplied by Gunn oscillators (90–150 GHz) and Schottky diode varactor multipliers. Some development is necessary to ensure adequate local oscillator power at the highest frequencies. The receivers will be mounted in a single dewar with a three-stage closed-cycle refrigerator having a capacity of 2.5 watts at 4.5K. Two of the eight receivers can be chosen for simultaneous observations, with some restrictions on possible pairs. However, the four receivers at 345 GHz and below will ensure that a low frequency receiver is always available in conjunction with one at high frequency to provide an astronomical phase reference. The two receivers at 345 GHz will be fed with orthogonal circular polarizations to provide for full polarization measurements (4 Stokes parameters) at that frequency.

The IF signal band will be 4–6 GHz, a frequency that provides a good balance between wide bandwidth and low noise figure. The IF signals as well as a signal from a reference source to phase lock the local oscillators will be transmitted by fiber optic cables. The stability of the best temperature compensated cables is $\sim 10^{-7}$ C^{-1} and it may not be necessary to build length stabilization systems. The phase stability of the cables when they are flexed in the antenna azimuth wrap is being studied.

7. CORRELATOR/SPECTROMETER

The correlator, the heart of the array's signal processing, will have a hybrid analog-digital design. A fully analog correlator would be useful only for wide-band continuum measurements, whereas a fully digital correlator could not be implemented to run fast enough at reasonable cost to cover the desired band of 2 GHz for spectral measurement. The solution is to build a hybrid signal processor in which the signals are bandlimited, converted to a convenient baseband, then passed to a digital correlator, and the results Fourier transformed into cross-power spectra. The bandwidth of the analog "chunks" should be large enough to reduce the number of seams in the total spectrum, yet small enough to keep the total cost reasonable.

The IF signals will consist of two 2 GHz bands from each antenna. These will be converted to 64 baseband chunks of 80 MHz bandwidth, spaced at 64 MHz intervals. The frequency conversion will be achieved with single sideband mixers which can be positioned anywhere in the band.

The digital correlator will be based on a full custom CMOS chip and board that is being developed at Haystack Observatory, Westerbork and SAO to satisfy the needs of the SMA, the NASA/MIT Mark IV VLBI processor, the Joint European VLBI processor and the Westerbork Array. The chip is being designed by the NASA VLSI Center at the University of New Mexico. The chip can generate a 512 lag correlation function from 2 bit (4 level) data at a maximum clock rate of 64 Msamples/sec. It will have 4 input channels, processed in 16 subsections of 32 lags

each, so that it can readily handle demultiplexed data. For the SMA application, an 80 MHz signal band will be demultiplexed by 4, and each chip will produce a 128-point correlation function. The chips can be daisy-chained to measure the cross correlator function over a wide range of delays. The chip also contains fringe rotators and other features for VLBI applications, which the SMA will not use.

The correlator will be very flexible in configuration. It will consist of 64 boards, each with 32 chips, and be capable of generating 262,144 baseline lags. With two 2 GHz bands and 15 baselines, one chip is required for each chunk and the resolution is 0.6 MHz (0.6 km/s at 300 GHz and 0.2 km/s at 850 GHz). If Hanning weighting is applied, the resolution would be 1.2 MHz. If polarization information is required, then two 2 GHz bands can be processed at 1.2 MHz resolution. For maximum spectral resolution, half the chips on each board can be applied to one bandwidth chunk to give 0.078 MHz resolution. Eight bandwidth chunks at arbitrary frequencies (e.g., 8 separate spectral lines) can be observed on all baselines at this spectral resolution. For an 8 element array (SMA, plus JCMT and CSO), one 2 GHz band can be processed on all 28 baselines. Many other modes will be possible.

The sampling interval is proportional to the ratio of resolution to the field of view or primary beam size. For the SMA, thirty seconds of sampling should be adequate. Hence the data rate is 131,000 complex samples/30 seconds, neglecting ancillary data, or 750 Mbyte/day.

I thank Ray Blundell, Colin Masson, and Eric Keto for helpful comments and Bernard Burke for pointing out the characteristics of Reauleux triangles to me.

References

Blundell, R. and Tong, C.-Y.E.: 1992, *P.I.E.E.E.* **80**, 1702

Cornwell, T.J.: 1988, *I.E.E.E. Trans. Antennas & Prop.* **36**, 1165

Gardner, M.: *The Unexpected Hanging and Other Mathematical Diversions*, *1968*, University of Chicago Press: Chicago, 212

Genzel, R.: in The Physics of Star Formation and Early Stellar Evolution, C.J. Lada and N.D. Kylafis, *1991*, Kluwer:Dordrecht, 155

Keto, E.: 1993, *I.E.E.E. Trans. Antennas & Prop.* **submitted**

Loeb, A.: 1993, *Ap.J.* **404**, L37

Masson, C.R.: 1993, *this volume*

Masson, C. R.: 1993a, in IAU Colloq. 140, Astronomy with Millimeter and Submillimeter Wave Interferometry, M. Ishiguro, ed(s)., *ASP:San Francisco, in press*

Masson, C.R. et al: 1992, in Design Study for the Submillimeter Interferometer Array of the SAO, ed(s)., *SAO Special Report*

Mezger, P.G., Chini, R., Kreysa, E., Wink, J.E., and Salter, C.J.: 1988, *Astr.Ap.* **191**, 44

Moran, J.M., Elvis, M.S., Fazio, G.C., Ho, P.T.P., Myers, P.C., Reid, M.J., and Willner, S.P.: 1984, in A Submillimeter Telescope Array, ed(s)., *SAO Special Report*

Phillips, T.G. and Keene, J.: 1992, *P.I.E.E.E.* **80**, 1662

Thompson, A.R., Moran, J.M., and Swenson, G.W.: 1986, *Interferometry and Synthesis in Radio Astronomy*, Wiley Interscience: New York

Welch, W.J.: 1993, in IAU Colloq. 140, Astronomy with Millimeter and Submillimeter Wave Interferometry, M. Ishiguro, ed(s)., *ASP:San Francisco, in press*

Discussion:

Burke:
Your "optimum" solution for antenna location places the elements on a Roulot triangle. Cornwell's "optimum" solution converged to location on a circle. Why the difference?
Moran:
The constraints were slightly different. Cornwell maximized the geometric mean distance among uv points.

Hall:
Considering the short baseline end of the phase fluctuation vs baseline plot, do you have an estimate for the intrinsic LO noise (say in degrees per hundred GHz) likely to contribute to the phase fluctuation residual?
Moran:
We are trying to design the LO system so that the coherence loss due to phase noise is less than 1% at the highest frequency of operation (800 GHz). This corresponds to about 1° rms phase noise per 100 GHz. The LO phase reference signal will be distributed at 6 GHz, making it easy to achieve relative phase stability. However we also plan to be able to use the array as a VLBI element.

Ekers:
In what sense is your configuration solution **optimum**?
Moran:
Within a circular boundary in the uv plane we sought the array configuration that gave the most uniform distribution of uv points.

https://doi.org/10.1017/S0074180900107296 Published online by Cambridge University Press